

---

# Vireo: Leveraging Depth and Language for Open-Vocabulary Domain-Generalized Semantic Segmentation

---

Siyu Chen<sup>1</sup>   Ting Han<sup>2†</sup>   Chengzheng Fu<sup>3\*</sup>   Changshe Zhang<sup>4\*</sup>   Chaolei Wang<sup>2\*</sup>  
Jinhe Su<sup>1</sup>   Guorong Cai<sup>1</sup>   Meiliu Wu<sup>5†</sup>

<sup>1</sup> Jimei University, <sup>2</sup> Sun Yat-sen University,

<sup>3</sup> Nanjing University of Aeronautics and Astronautics, <sup>4</sup> Xidian University, <sup>5</sup> University of Glasgow

## Abstract

Open-Vocabulary semantic segmentation (OVSS) and domain generalization in semantic segmentation (DGSS) highlight a subtle complementarity that motivates Open-Vocabulary Domain-Generalized Semantic Segmentation (OV-DGSS). OV-DGSS aims to generate pixel-level masks for unseen categories while maintaining robustness across unseen domains, a critical capability for real-world scenarios such as autonomous driving in adverse conditions. We introduce **Vireo, a novel single-stage framework for OV-DGSS that unifies the strengths of OVSS and DGSS for the first time.** Vireo builds upon the frozen Visual Foundation Models (VFM) and incorporates scene geometry via Depth VFM to extract domain-invariant structural features. To bridge the gap between visual and textual modalities under domain shift, we propose three key components: (1) GeoText Prompts, which align geometric features with language cues and progressively refine VFM encoder representations; (2) Coarse Mask Prior Embedding (CMPE) for enhancing gradient flow for faster convergence and stronger textual influence; and (3) the Domain-Open-Vocabulary Vector Embedding Head (DOV-VEH), which fuses refined structural and semantic features for robust prediction. Comprehensive evaluation on these components demonstrates the effectiveness of our designs. Our proposed Vireo achieves the **state-of-the-art performance and surpasses existing methods by a large margin** in both domain generalization and open-vocabulary recognition, offering a unified and scalable solution for robust visual understanding in diverse and dynamic environments. Code is available at <https://github.com/anonymouse-9c53tp182bvz/Vireo>.

## 1 Introduction

Open-Vocabulary Domain-Generalized Semantic Segmentation (OV-DGSS) denotes the joint execution of open-vocabulary semantic segmentation (OVSS)[1, 2, 3, 4] and domain generalization in semantic segmentation (DGSS)[5, 6, 7, 8] tasks. It involves training a model that, without access to target-domain samples or annotations for novel categories, can generate pixel-wise segmentation for unseen classes while sustaining high performance across previously unseen domains (such as different cities, lighting environments, or climatic conditions). For instance, when an autonomous vehicle receives a query like “Can I park next to that bollard?”, its perception system must comprehend the linguistic input and accurately segment the referenced object at the pixel level—even under adverse conditions such as dim lighting, rain-streaked lenses, or region-specific visual appearances.

OVSS and DGSS share notable similarities and can both be implemented using either multi-stage or single-stage strategies. In multi-stage OVSS [1], candidate regions or coarse masks are generated and

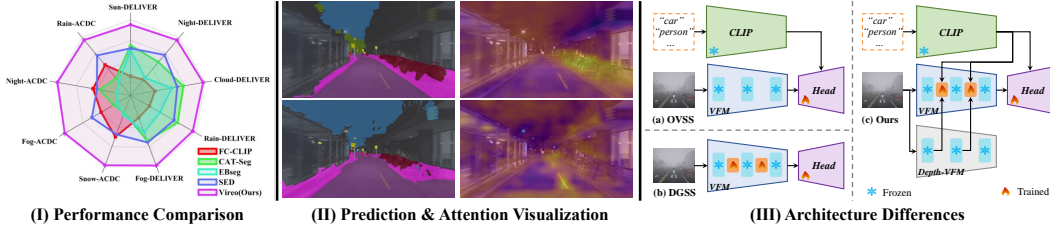


Figure 1: **Overview of Vireo and effectiveness.** (I) Performance comparison under various adverse conditions across ACDC and DELIVER datasets, showing that Vireo consistently outperforms existing methods. (II) Qualitative visualization of segmentation predictions (left) and attention maps (right) under extreme night scenes, illustrating Vireo’s robustness and precise alignment with semantic cues. (III) Architectural comparison: (a) Traditional OVSS and (b) DGSS pipelines freeze or fine-tune VFM separately without cross-modal integration; (c) Our proposed Vireo introduces GeoText Prompts and Depth-VFM integration to enhance both semantic alignment and domain robustness.

then classified by a text approach, while multi-stage DGSS [9] first aligns domains through adversarial alignment or style transfer and then trains the segmentation approach on the aligned features.

In single-stage OVSS [10, 11], the segmentation head is dynamically conditioned on text prompts to directly produce masks for each class. In contrast, single-stage DGSS [12, 13] incorporates domain-invariant modules within the backbone or segmentation head, enabling the model to jointly learn segmentation and generalization in a unified forward pass without requiring distinct stages. The key distinction lies in their focus: OVSS requires integration of visual features with textual semantics to accurately identify unseen classes, whereas DGSS emphasizes robustness to domain shifts.

Consequently, integrating open-vocabulary recognition of novel classes with domain robustness into a unified framework presents two primary challenges: (1) *Text-vision alignment modules often degrade outside the source domain, leading to significant performance drops even for previously seen classes.* (2) *Domain-invariant strategies may suppress fine-grained semantic cues, hindering the model’s ability to precisely respond to detailed textual queries.*

Recent single-stage DGSS studies have increasingly adopted strategies that fine-tune learnable tokens across the layers of a frozen Visual Foundation Model (VFM) [14, 15, 16, 17, 18] to adapt its feature representations. In OVSS, the VFM encoder is typically fully frozen, with efforts focused on designing the decoder to endow the model with open-vocabulary recognition capabilities. This reveals a subtle complementarity between the two paradigms: **DGSS emphasizes the encoder by leveraging the VFM’s strong feature generalization to learn cross-domain representations, whereas OVSS freezes the encoder and emphasizes the decoder to enable open-vocabulary recognition.**

Moreover, in cross-domain scenarios, depth and geometric cues are largely insensitive to variations in illumination and texture [19, 20]. They supply reliable spatial constraints, easing the distribution shift of RGB features and sharpening boundary localization. Recent studies such as DepthForge [21] have shown that injecting depth prompts into a frozen VFM boosts domain generalization. Motivated by these findings, we adopt DepthAnything V2 as our Depth VFM: its diverse pre-training delivers consistent depth estimation across domains, and keeping it fully frozen incurs minimal training cost while preserving real-time inference speed.

In this paper, we propose a VFM-based single-stage pipeline for OV-DGSS, termed **Vireo**. Specifically, in the encoder, both the VFM and DepthAnything modules are kept frozen. The VFM is leveraged to robustly capture cross-domain visual features, while DepthAnything extracts the scene’s intrinsic geometric structure. On this basis, we introduce **Geometric-Text Prompts (GeoText Prompts)** to fuse the extracted structural features with manually provided textual cues, progressively refining the feature maps between the frozen VFM layers. To mitigate the slow convergence caused by sparse gradients propagating through the frozen encoder, we introduce a **Coarse Mask Prior Embedding (CMPE)** at the beginning of the decoder to inject denser gradient signals. This design accelerates the convergence of mask supervision and further strengthens the influence of textual priors. Subsequently, we design the **Domain-Open-Vocabulary Vector Embedding Head (DOV-VEH)** to strengthen the synergistic integration of structural and textual modalities, ensuring that both cross-domain structural features and open-vocabulary cues learned by the GeoText prompts are fully utilized in the final prediction.



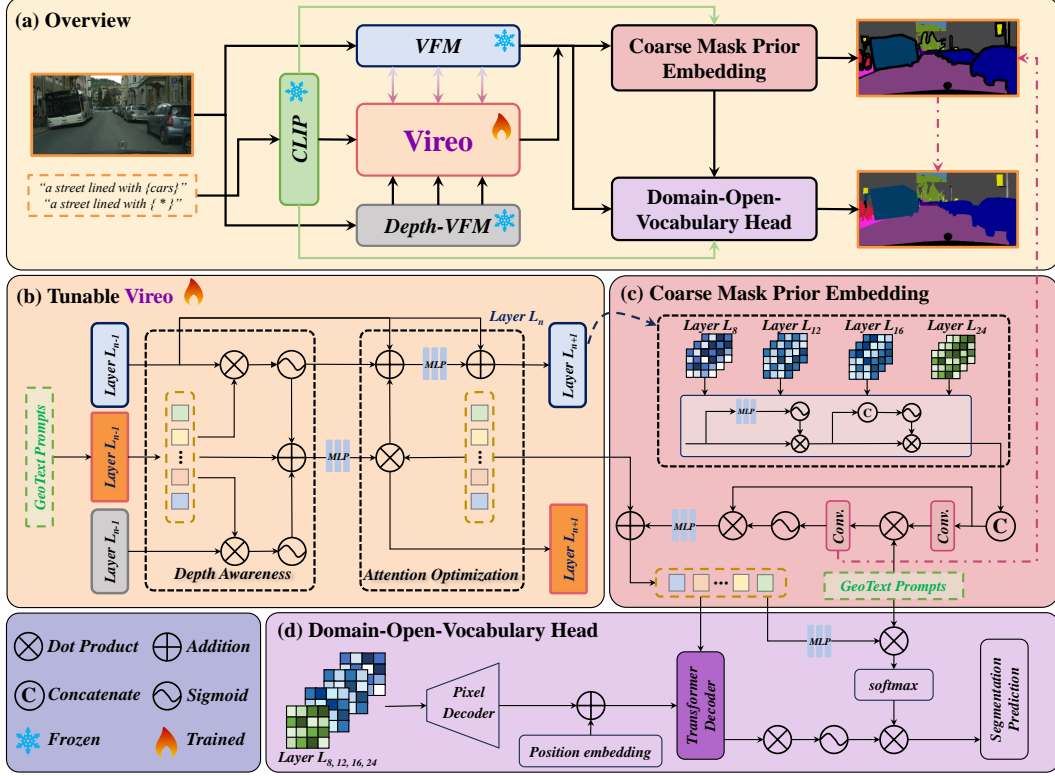


Figure 2: **Overview of the proposed Vireo framework for OV-DGSS.** (a) **Framework Overview.** Geometric-Text Prompts permeate our model: they’re injected in Tunable Vireo to align domain priors, reused in CMPE to guide multi-scale feature fusion, and employed in DOV-VEH as queries for open-vocabulary segmentation, forming a unified end-to-end loop. (b) **Tunable Vireo.** GeoText Prompts are used to inject structural-textual priors across multiple layers. Depth-aware fusion and attention optimization are applied between intermediate frozen layers to progressively refine representations. (c) **Coarse Mask Prior Embedding (CMPE).** Multi-scale features from VFM are combined with GeoText Prompts to provide dense supervision and gradient signals for downstream modules. (d) **Domain-Open-Vocabulary Head (DOV-VEH).** Multi-level features are processed by a Pixel Decoder and Transformer Decoder to produce final predictions guided by open-vocabulary text queries.

**For challenge 1:** We find that GeoText Prompts not only capture structural and semantic cues within the frozen VFM encoder but also guide the progressive refinement of its feature representations.

**For challenge 2:** The CMPE enhances gradient back-propagation into the encoder, while the redesigned DOV-VEH deepens the fusion of visual and textual priors. These components form a unified framework that simultaneously achieves domain robustness and strong open-vocabulary generalization. Our main contributions are summarized as follows:

- (1) We propose **Vireo**, a novel VFM-based single-stage framework for OV-DGSS.
- (2) We introduce **GeoText Prompts** to progressively refine frozen VFM features by injecting geometric cues from DepthAnything and aligning them with textual semantics, enabling structural-semantic fusion across encoder layers.
- (3) We design two complementary modules—**CMPE** for enhancing gradient flow and **DOV-VEH** for fusing visual and textual priors—together boosting segmentation performance under domain shifts and unseen classes.

## 2 Related Works

**Open-Vocabulary Semantic Segmentation.** Open-Vocabulary Semantic Segmentation (OVSS) aims to segment objects based on arbitrary textual descriptions, moving beyond fixed, pre-defined

categories. A key enabler for OVSS [22, 23, 1, 24] has been vision-language models (VLMs), particularly CLIP [16], which aligns visual and textual representations.

**Domain-Generalized Semantic Segmentation.** Domain Generalization in Semantic Segmentation (DGSS) addresses the performance degradation when models encounter unseen target domains due to domain shift—variations in data distributions (e.g., lighting, weather). Data augmentation [25, 26] and learning domain-invariant representations [27, 28] are two key strategies to enhance model robustness. This detailed discussion in the appendix further contextualizes our specific contributions within the broader landscape of these research areas.

### 3 Methodology - Vireo

#### 3.1 Overview

As illustrated in Figure 2, our framework consists of three key modules tailored for the OV-DGSS:

- **Tunable Vireo with GeoText Prompts:** Introduces GeoText Prompts to inject and refine both geometric and textual information across layers of a frozen VFM.
- **Coarse Mask Prior Embedding (CMPE):** Generates coarse prior masks to guide segmentation and reinforce gradient flow from the decoder back to the frozen encoder.
- **Domain-Open-Vocabulary Vector Embedding Head (DOV-VEH):** Integrates visual, geometric, and semantic features to produce final OV-DGSS predictions.

The input RGB image  $I \in \mathbb{R}^{H \times W \times 3}$  is duplicated and independently fed into two frozen encoders: a VFM encoder  $\mathcal{F}^V$  and a DepthAnything encoder  $\mathcal{F}^D$ . These backbones extract a series of multi-scale features  $f_l^V$  and  $f_l^D$  respectively, where  $l$  denotes the encoder layer index in  $[1, L]$ . In parallel, a set of class labels  $\mathcal{C} = \{c_1, \dots, c_K\}$  is transformed into natural language prompts  $T = \{\text{prompt}_1, \dots, \text{prompt}_K\}$ , which are encoded using a frozen CLIP text encoder  $\mathcal{F}^T$  to obtain textual embeddings  $t_k \in \mathbb{R}^d$ . These features serve as shared semantic priors across the entire framework and are precomputed once at initialization. In the Tunable Vireo module, each layer receives a tuple  $(f_l^V, f_l^D, t_k)$ , and applies the GeoText Prompts  $P_l$  to align and refine the visual features. This is achieved by computing cross-modal attention maps  $\mathcal{A}_l = \text{Attn}(P_l, f_l^V, f_l^D, t_k)$  followed by feature fusion and projection. The refined output  $\hat{f}_l^V$  is then forwarded back to update the VFM’s layer-wise activations.

We select the refined visual features  $\{f_{l_i}^V\}_{i=1}^4$  from the VFM encoder at layers  $l_1 = 8$ ,  $l_2 = 12$ ,  $l_3 = 16$ , and  $l_4 = 24$  for downstream decoding. In the Coarse Mask Prior Embedding (CMPE) module, these features are first upsampled to a unified spatial resolution and passed through a channel-spatial attention gating function  $\mathcal{G}(\cdot)$ . The gated outputs are then fused to form a global coarse feature  $f^M \in \mathbb{R}^d$ . The  $f^M$  is projected and matched with the text embeddings  $t_k \in \mathbb{R}^d$  to produce a coarse class probability map  $\mathcal{M} \in \mathbb{R}^{H \times W \times K}$ , where  $\mathcal{M}$  serves both as a weak supervision signal and as a prior to construct the query embeddings  $\mathcal{Q}$ . The query prior is added to the GeoText Prompts and forwarded to the final segmentation head. In the Domain-Open-Vocabulary Vector Embedding Head (DOV-VEH), the multi-scale features  $\{\hat{f}_{l_i}^V\}_{i=1}^4$  are passed through a pixel decoder  $\mathcal{D}_p(\cdot)$  to enhance spatial representation, followed by a Transformer decoder  $\mathcal{D}_T(\cdot)$  that leverages positional embedding. The GeoText Prompts serve as learnable queries and interact with both the decoded features and the text embeddings, producing pixel-level mask embeddings  $\mathcal{E}_{\text{mask}}(x, y) \in \mathbb{R}^d$  and classification embeddings  $\mathcal{E}_{\text{cls}}(k) \in \mathbb{R}^d$ . The final prediction is  $\hat{\mathcal{M}}(x, y, k) \in \mathbb{R}^{H \times W \times K}$  provides the pixel-wise semantic prediction with both fine-grained detail and open-vocabulary generalization capability.

#### 3.2 Tunable Vireo with GeoText Prompts

To improve efficiency, we first precompute and share the textual prompt embeddings using a frozen CLIP text encoder  $\mathcal{F}^T$ . Specifically, a set of class labels  $\mathcal{C} = \{c_1, \dots, c_K\}$  is transformed into language prompts  $T = \{\text{prompt}_1, \dots, \text{prompt}_K\}$ , which are encoded as  $t_k = \mathcal{F}^T(\text{prompt}_k)$ , where  $t_k \in \mathbb{R}^d$ . These embeddings are reused across all GeoText Prompt layers, CMPE, and DOV-VEH modules to avoid redundant computation.

During inference, the input image  $I \in \mathbb{R}^{H \times W \times 3}$  is simultaneously processed by a frozen visual encoder  $\mathcal{F}^V$  and a frozen depth encoder  $\mathcal{F}^D$  (e.g., DepthAnything). For each selected layer  $l \in \{1, \dots, L\}$ , we obtain the visual feature map  $f_l^V = \mathcal{F}_l^V(I)$  and the depth feature map  $f_l^D = \mathcal{F}_l^D(I)$ . Each layer of the Tunable Vireo module receives the tuple  $(f_l^V, f_l^D, \{t_k\})$  along with a layer-specific GeoText Prompt  $P_l \in \mathbb{R}^{N \times d}$ , where  $N$  is the number of learnable prompts.

The prompt  $P_l$  first interacts with the textual embeddings via a fusion block, then attends to both  $f_l^V$  and  $f_l^D$  through cross-attention mechanisms:

$$\mathcal{A}_l = \text{CrossAttn}(P_l, f_l^V, f_l^D, \{t_k\}). \quad (1)$$

The attention outputs are fused via weighted summation, then passed through an MLP projection layer and multiplied element-wise with  $P_l$ . A residual connection adds this result to the original feature map  $f_l^V$ , yielding a refined visual representation  $\hat{f}_l^V$ . Finally, another MLP transforms  $\hat{f}_l^V$  into the input for the next VFM layer, and the updated GeoText Prompt  $P_{l+1}$  is passed forward.

This progressive refinement continues across all selected layers, enabling the model to inject and align geometric and semantic information at multiple scales, thereby enhancing cross-domain robustness and open-vocabulary generalization.

### 3.3 Coarse Mask Prior Embedding (CMPE)

We select the refined visual features  $\{\hat{f}_{l_i}^V\}_{i=1}^4$  from the VFM encoder at layers  $l_1 = 8$ ,  $l_2 = 12$ ,  $l_3 = 16$ , and  $l_4 = 24$ , respectively. Each feature map is upsampled to a common spatial resolution  $(H \times W)$  via bilinear interpolation, and then passed through an Adaptive Attention Gate (AAG)  $\mathcal{G}(\cdot)$ , which enhances informative channels and spatial regions. Specifically, AAG applies two  $1 \times 1$  convolutions followed by ReLU and Sigmoid for channel attention, and a  $3 \times 3$  convolution followed by Sigmoid for spatial attention.

The attended features are concatenated along the channel axis and fused via a  $1 \times 1$  convolution to restore the embedding dimension  $d$ , yielding a fused feature representation:  $f^M = \text{Fuse}(\mathcal{G}(\hat{f}_{l_i}^V))$ . We apply a residual addition between  $f^M$  and the final layer output  $\hat{f}_{l_4}^V$  to obtain the updated mask feature:  $f^M = f^M + \hat{f}_{l_4}^V$ . This fused feature  $f^M(x, y) \in \mathbb{R}^d$  is projected to the same dimension as the text embeddings  $t_k \in \mathbb{R}^d$  and compared via Einstein summation to generate a coarse semantic probability map  $\mathcal{M}(x, y, k) = \langle f^M(x, y), t_k \rangle$ , where  $\mathcal{M} \in \mathbb{R}^{B \times K \times H \times W}$ . This coarse mask is supervised with a segmentation loss to enhance gradient flow through the frozen encoder.

To generate query priors for the downstream segmentation head, we first normalize  $\mathcal{M}$  across the spatial domain to derive attention weights:

$$\alpha_k(x, y) = \frac{\exp(\mathcal{M}(x, y, k))}{\sum_{x', y'} \exp(\mathcal{M}(x', y', k))}. \quad (2)$$

Then, we compute the class-specific aggregated feature by spatially weighting  $f^M$ :

$$f_k^{\text{class}} = \sum_{x, y} \alpha_k(x, y) \cdot f^M(x, y). \quad (3)$$

Each  $f_k^{\text{class}}$  is projected into the embedding space as  $e_k^{\text{class}} \in \mathbb{R}^d$ , and combined with a set of learnable query vectors  $\{q_j\}_{j=1}^{N_q}$  to produce the query priors:

$$q_j^{\text{prior}} = \sum_{k=1}^K \text{Softmax}(\langle q_j, e_k^{\text{class}} \rangle) \cdot e_k^{\text{class}}. \quad (4)$$

The final query priors  $\{q_j^{\text{prior}}\}_{j=1}^{N_q}$  are added to the corresponding GeoText Prompts and forwarded into the Domain-Open-Vocabulary Vector Embedding Head (DOV-VEH).

### 3.4 Domain-Open-Vocabulary Vector Embedding Head (DOV-VEH)

The DOV-VEH module receives the refined multi-scale features  $\{\hat{f}_{l_i}^V\}_{i=1}^4$  from the VFM encoder, where  $l_1 = 8$ ,  $l_2 = 12$ ,  $l_3 = 16$ , and  $l_4 = 24$ , along with the updated GeoText Prompts  $\{P_l\}$ . These

Table 1: Performance comparison between our Vireo and existing OVSS and DGSS methods under *Citys.*  $\rightarrow$  *ACDC* + *BDD.* + *Map.*, and *GTA5.*  $\rightarrow$  *Citys.* + *BDD.* + *Map.* generalization settings. Top three results are highlighted as **best**, **second**, and **third**, respectively. (%)

Method	Proc. & Year	Trained on Cityscapes						Trained on GTA5			
		Night-ACDC	Fog-ACDC	Rain-ACDC	Snow-ACDC	BDD 100k	Mapillary	GTA5	Cityscapes	BDD100k	Mapillary
OVSS Method											
FC-CLIP [29]	NeurIPS2023	40.8	64.4	63.2	61.5	55.92	66.12	47.12	53.54	51.41	58.60
EBSeg [30]	CVPR2024	27.7	56.5	51.8	50.1	48.91	63.40	42.61	44.80	40.59	56.28
CAT-Seg [10]	CVPR2024	37.2	58.3	45.6	49.0	48.26	54.74	45.18	43.52	44.28	50.88
SED [3]	CVPR2024	38.7	69.0	56.4	60.2	53.30	64.32	48.93	47.45	48.16	57.38
DGSS Method											
ResNet based:											
IBN [31]	ECCV2018	21.2	63.8	50.4	49.6	48.56	57.04	45.06	-	-	-
RobustNet [9]	CVPR2021	24.3	64.3	56.0	49.8	50.73	58.64	45.00	36.58	35.20	40.33
WildNet [32]	CVPR2022	12.7	41.2	34.2	28.4	50.94	58.79	47.01	44.62	38.42	46.09
Transformer based:											
HGFormer [33]	CVPR2023	52.7	69.9	72.0	68.6	53.40	66.90	51.30	-	-	-
CMFormer [34]	AAAI2024	33.7	77.8	67.6	64.3	59.27	71.10	58.11	55.31	49.91	60.09
VFM based:											
REIN [35]	CVPR2024	55.9	79.5	72.5	70.6	63.54	74.03	62.41	66.40	60.40	66.10
FADA [36]	NeurIPS2024	57.4	80.2	75.0	73.5	65.12	75.86	63.78	68.23	61.94	68.09
OV-DGSS Method											
Vireo (Ours)	-	60.6	82.3	76.3	76.2	66.73	75.99	67.86	70.69	62.91	69.63

features are first processed by a pixel decoder  $\mathcal{D}_p(\cdot)$ , which leverages multi-scale cross-attention to extract rich spatial context:  $f^{\text{pix}} = \mathcal{D}_p(\hat{f}_{l_i}^V)$ . The fused feature  $f^{\text{pix}} \in \mathbb{R}^{H \times W \times d}$  is then compressed via a  $1 \times 1$  convolution and enriched with sinusoidal positional encoding to preserve spatial structure.

The enhanced features are fed into a Transformer Decoder  $\mathcal{D}_T(\cdot)$ , where the GeoText Prompts act as learnable queries. Through stacked layers of self-attention and cross-attention with  $f^{\text{pix}}$ , the model captures fine-grained visual-semantic alignment, yielding a set of high-resolution mask features  $\mathcal{E}_{\text{mask}}(x, y) \in \mathbb{R}^d$  at each spatial position.

Simultaneously, the GeoText Prompts  $\{P\}$  are passed through a two-layer MLP and then interact with the text embeddings  $\{t_k\}$  (precomputed from the CLIP text encoder) to produce classification-level representations  $\mathcal{E}_{\text{cls}}(k) \in \mathbb{R}^d$ . The final segmentation prediction  $\hat{\mathcal{M}} \in \mathbb{R}^{H \times W \times K}$  is generated via an Einstein summation over the two embeddings:

$$\hat{\mathcal{M}}(x, y, k) = \sum_{d=1}^D \mathcal{E}_{\text{mask}}(x, y, d) \cdot \mathcal{E}_{\text{cls}}(k, d), \quad (5)$$

where  $D$  is the feature embedding dimension. This design enables DOV-VEH to generate pixel-level segmentation masks that are both spatially accurate and semantically aligned with open-vocabulary textual queries.

## 4 Experiments

### 4.1 Datasets & Evaluation Protocols

We evaluate Vireo on six real-world datasets (**Cityscapes** [37], **BDD100K** [38], **Mapillary** [39], **ACDC** [40], **ADE150** [41], and **ADE847** [41]) and two synthetic datasets (**GTA5** [42] and **DELIVER** [43]). **Cityscapes** (City.) is an autonomous-driving dataset with 2,975 training images and 500 validation images, each at a resolution of  $2048 \times 1024$ . **BDD100K** (BDD.) and **Mapillary** (Map.) provide 1,000 and 2,000 validation images, respectively, at resolutions of  $1280 \times 720$  and  $1920 \times 1080$ . **ACDC** offers 406 validation images captured under extreme conditions (night, snow, fog, and rain), each at  $1920 \times 1080$ . **GTA5** is a synthetic dataset that contains 24,966 labeled images obtained from a video game. **DELIVER** is a multimodal synthetic dataset comprising 3,983 training images, 2,005 validation images, and 1,897 test images across five weather conditions (cloudy, foggy, night, rainy, and sunny); every image is  $1042 \times 1042$  and there are 25 classes. **ADE150** and **ADE847** refer to subsets of the ADE20K dataset [41], each containing 2,000 validation images of variable resolution sourced from diverse scenes such as SUN and Places, covering 150 and 847 semantic categories, respectively.

Following the existing DGSS evaluation protocol, we train on one dataset as the source domain and validate on multiple unseen target domains. The three standard evaluation setups are: (1) Cityscapes  $\rightarrow$  ACDC; (2) GTA5  $\rightarrow$  Cityscapes, BDD100K, Mapillary; (3) Cityscapes  $\rightarrow$  BDD100K, Mapillary, GTA5. To assess our proposed OV-DGSS approaches and compare its open-vocabulary capability

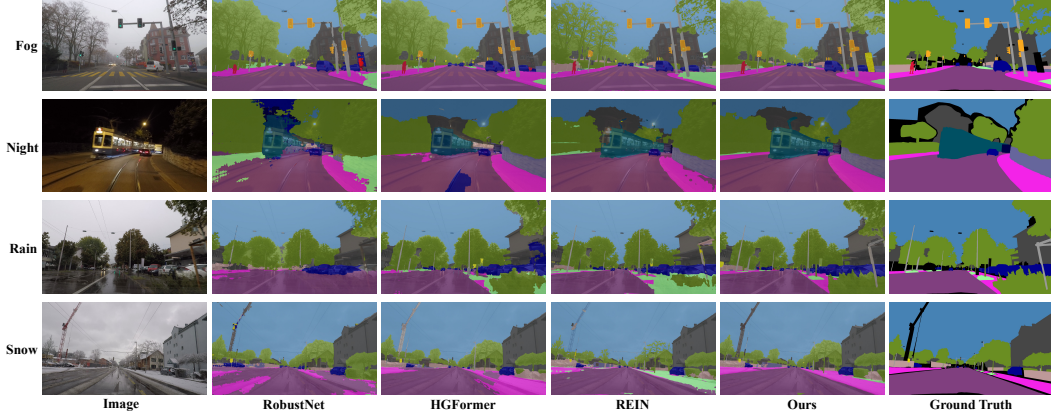


Figure 3: Key segmentation examples of existing DGSS methods and Vireo under the Cityscapes  $\rightarrow$  ACDC unseen target domains under Night, Snow, Rain, and Fog conditions.

Table 2: Performance comparison between our Vireo and existing OVSS methods under Cityscapes  $\rightarrow$  DELIVER + Ade150 + Ade847 generalization setting. Top three results are highlighted as **best**, **second**, and **third**, respectively. (%)

Method	Proc. & Year	Sun-DELIVER	Night-DELIVER	Cloud-DELIVER	Rain-DELIVER	Fog-DELIVER	Ade150	Ade847
<b>Train on Cityscapes</b>								
<i>OVSS Method:</i>								
FC-CLIP [29]	NeurIPS2023	16.93	14.93	17.50	16.59	17.26	16.12	6.29
EBSeg [30]	CVPR2024	26.41	15.50	22.62	20.35	22.00	12.75	3.75
CAT-Seg [10]	CVPR2024	28.21	20.56	26.22	26.53	24.80	20.19	6.95
SED [3]	CVPR2024	27.14	22.79	24.40	25.18	25.25	18.86	5.45
<i>OV-DGSS Method:</i>								
<b>Vireo (Ours)</b>	–	<b>35.73</b>	<b>27.51</b>	<b>32.34</b>	<b>31.80</b>	<b>32.72</b>	<b>21.37</b>	<b>7.31</b>
<b>Train on GTA</b>								
<i>OVSS Method:</i>								
FC-CLIP [29]	NeurIPS2023	22.24	18.58	18.50	16.59	19.12	15.47	5.73
EBSeg [30]	CVPR2024	32.32	20.05	26.19	26.19	28.69	11.87	4.19
CAT-Seg [10]	CVPR2024	28.59	23.49	27.31	27.94	27.66	20.45	7.18
SED [3]	CVPR2024	26.56	21.18	24.95	24.58	26.17	19.57	6.80
<i>OV-DGSS Method:</i>								
<b>Vireo (Ours)</b>	–	<b>38.49</b>	<b>29.89</b>	<b>33.89</b>	<b>33.46</b>	<b>35.80</b>	<b>21.23</b>	<b>7.68</b>

against OVSS approaches, we additionally introduce two more configurations: (4) Cityscapes  $\rightarrow$  DELIVER, ADE150, ADE847; (5) GTA5  $\rightarrow$  DELIVER, ADE150, ADE847. The evaluation metric is mean Intersection over Union (mIoU).

## 4.2 Deployment Details & Parameter Settings

Our implementation is built upon the MMSegmentation [44] codebase. We employ the AdamW optimizer with an initial learning rate of  $1e-4$ , a weight decay of 0.05, epsilon set to  $1e-8$ , and beta parameters of (0.9, 0.999). The total number of training iterations is 40,000, matching REIN, and we adopt a polynomial learning-rate decay schedule that reduces the learning rate to zero over 40,000 iterations with a decay power of 0.9 and no epoch-based warmup. Data augmentation comprises multi-scale resizing, random cropping (with fixed crop size and category-ratio constraint), random horizontal flipping, and photometric distortion. All experiments are conducted on an NVIDIA RTX A6000 GPU with a batch size of 8, taking approximately 14 hours to train and peaking at around 45 GB of GPU memory usage.

## 4.3 Performance Comparison

**Domain Generalization Ability:** Table 1 summarizes the evaluation results of various state-of-the-art open-vocabulary semantic segmentation (OVSS) and domain-generalized semantic segmentation (DGSS) methods under two cross-domain settings (Cityscapes  $\rightarrow$  ACDC, BDD100k, Mapillary, GTA5 and GTA5  $\rightarrow$  Cityscapes, BDD100k, Mapillary). The results demonstrate that our approach achieves outstanding performance across all target datasets, significantly outperforming other OVSS/DGSS methods. Furthermore, the visualizations in Figure 3 shows that Vireo delivers



Table 3: Comparison of Seen and Unseen Category mIoU Across Weather Scenarios and Methods.

Class	Cloud					Fog					Night					Rain					Sun				
	Ours	SED	CAT-Seg	FC-CLIP	EBSeg	Ours	SED	CAT-Seg	FC-CLIP	EBSeg	Ours	SED	CAT-Seg	FC-CLIP	EBSeg	Ours	SED	CAT-Seg	FC-CLIP	EBSeg	Ours	SED	CAT-Seg	FC-CLIP	EBSeg
Seen	49.14	36.72	43.92	28.07	38.10	49.59	38.28	41.43	26.06	35.76	41.63	34.99	34.89	23.03	26.03	47.15	37.35	41.43	25.59	31.96	55.16	41.68	45.10	26.52	42.63
Unseen	10.96	8.74	3.69	4.05	2.92	12.15	8.40	3.54	4.32	4.48	9.52	7.27	2.30	4.09	2.09	12.27	8.95	5.81	4.60	5.57	11.46	8.12	4.91	4.73	6.14
Mean	33.89	24.40	26.22	17.50	22.62	35.80	25.25	24.80	17.26	22.00	29.89	22.79	20.56	14.93	15.50	33.46	25.18	26.53	16.59	20.35	38.49	27.14	28.21	16.93	26.41

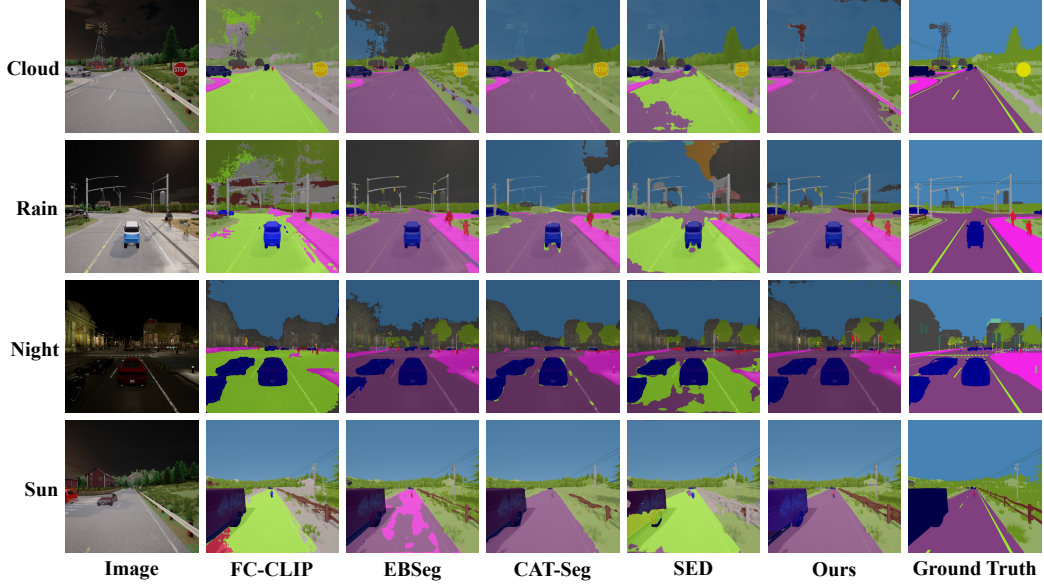


Figure 4: Key segmentation examples of existing OV-DGSS methods comparison on unseen classes and cross domain on Cityscapes → DELIVER.

satisfactory predictions in both extreme weather conditions and scenes with dense pedestrian and vehicular traffic.

**Open-Vocabulary Capability:** Table 2 presents a comparison between Vireo and other open-vocabulary semantic segmentation (OVSS) methods under the Cityscapes → DELIVER (sun, rain, night, cloud, fog), ADE150, and ADE847 configurations. The results indicate that conventional OVSS approaches suffer a sharp performance drop in extreme scenarios (e.g., night), whereas our model—enhanced by depth-based geometric features—maintains robust performance, outperforming the strongest OVSS baseline by at least 5%. Furthermore, as shown in Figure 4, the coexistence of new open classes and extreme weather conditions in the DELIVER dataset leads OVSS approaches to exhibit significant false positives and false negatives.

Table 3 compares Vireo trained on Cityscapes with other open-vocabulary semantic-segmentation methods on the DELIVER dataset across five weather conditions for both Seen and Unseen categories. Vireo achieves the highest mIoU for both groups: it outperforms the second-best method by roughly 7–10 percentage points on Seen classes and by 2–3 points on Unseen ones. Although all methods register lower mIoU on Unseen categories—underscoring the difficulty of open-vocabulary segmentation—Vireo substantially reduces this gap, confirming that its depth-geometry guidance and cross-domain alignment improve recognition of new classes. Overall, Vireo remains consistently superior across weather scenarios and category types, demonstrating stronger out-of-domain generalization.

#### 4.4 Ablation Study

**Robust Performance Gains.** In Table 4, we compare parameter overhead and mIoU of lightweight tuning methods on EVA02-Large and DINOv2-Large under the GTA5 → Cityscapes + BDD + Mapillary transfer. With only  $\approx 3.8$  M trainable parameters, Vireo leads both: 66.0% on EVA02 (+1.1% over FADA) and 67.7% on DINOv2 (+1.6%). Other schemes (REIN, LoRA, VPT, AdaptFormer)

Table 4: Performance comparison of the proposed **Vireo** against other DGSS methods under the  $GTA5 \rightarrow Citys.+BDD.+Map.$  setting.

EVA02 (Large) [45, 46]						DINOv2 (Large) [53]					
Fine-tune Method	Trainable Params*	mIoU			Avg.	Fine-tune Method	Trainable Params*	mIoU			Avg.
		Citys.	BDD.	Map.				Citys.	BDD.	Map.	
Full	304.24M	62.1	56.2	64.6	60.9	Full	304.20M	63.7	57.4	64.2	61.7
+AdvStyle[47]	304.24M	63.1	56.4	64.0	61.2	+AdvStyle[47]	304.20M	60.8	58.0	62.5	60.4
+PASTA[48]	304.24M	61.8	57.1	63.6	60.8	+PASTA[48]	304.20M	62.5	57.2	64.7	61.5
+GTR-LTR[49]	304.24M	59.8	57.4	63.2	60.1	+GTR-LTR[49]	304.20M	62.7	57.4	64.5	61.6
Freeze	0.00M	56.5	53.6	58.6	56.2	Freeze	0.00M	63.3	56.1	63.9	61.1
+AdvStyle[47]	0.00M	51.4	51.6	56.5	53.2	+AdvStyle[47]	0.00M	61.5	55.1	63.9	60.1
+PASTA[48]	0.00M	57.8	52.3	58.5	56.2	+PASTA[48]	0.00M	62.1	57.2	64.5	61.3
+GTR-LTR[49]	0.00M	52.5	52.8	57.1	54.1	+GTR-LTR[49]	0.00M	60.2	57.7	62.2	60.0
+LoRA[50]	1.18M	55.5	52.7	58.3	55.5	+LoRA[50]	0.79M	65.2	58.3	64.6	62.7
+AdaptFormer[51]	3.17M	63.7	59.9	64.2	62.6	+AdaptFormer[51]	3.17M	64.9	59.0	64.2	62.7
+VPT[52]	3.69M	62.2	57.7	62.5	60.8	+VPT[52]	3.69M	65.2	59.4	65.5	63.3
+REIN[35]	2.99M	65.3	60.5	64.9	63.6	+REIN[35]	2.99M	66.4	60.4	66.1	64.3
+FADA[36]	11.65M	66.7	61.9	66.1	64.9	+FADA[36]	11.65M	68.2	62.0	68.1	66.1
+Vireo (Ours)	3.78M	68.5	62.1	67.4	66.0	+Vireo (Ours)	3.78M	70.7	62.9	69.6	67.7

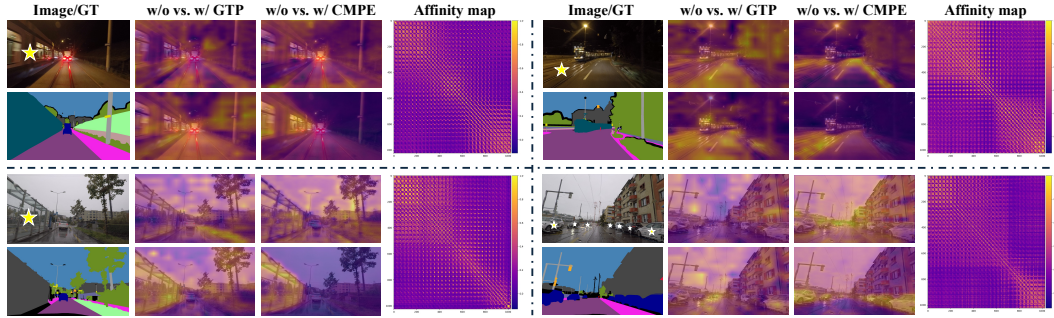


Figure 5: Visualizations of attention maps and affinity maps under different scenes, where CMPE denotes the Coarse Mask Prior Embedding, GTP represents the GeoText Prompts, respectively.

improve a frozen backbone but fall short of Vireo’s accuracy-efficiency balance. Versus full fine-tuning, Vireo slashes training cost and further improves mIoU, showing its depth-geometry prompts generalize across VFMs.

Table 6 reports the parameter overhead and mIoU of Vireo and several lightweight fine-tuning schemes on four backbones (CLIP-L, SAM-H, EVA02-L, and DINOv2-L). Compared with the prompt-based REIN baseline, Vireo adds only about 0.79 M extra parameters yet achieves the highest average mIoU on every backbone: the gain is most pronounced on the parameter-constrained CLIP-L, and Vireo still surpasses heavier adapters such as FADA by 1–2 mIoU on the larger EVA02-L and DINOv2-L models, underscoring its parameter efficiency and scalability across backbones.

In Table 5, using Depth Anything V2 alone yields an approximate 0.6% mIoU gain across all six scenarios, and adding depth augmentation with attention optimization (DA + AO) delivers a further  $\approx 1\%$  improvement. The DOV-VEH and CMPE modules each add 0.5%–0.8%, validating mask vectors and dense gradient embedding. GeoText Prompts on its own provides a substantial  $\approx 4.4\%$  boost, underscoring the complementary benefits of fusing semantic and geometric cues.

**Pronounced Attention Focus.** Figure 5 further confirm that GeoText Prompts steer the model toward geometry-sensitive regions, while CMPE strengthens gradients on

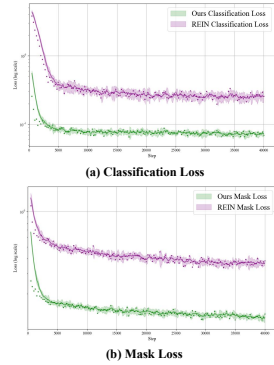


Figure 7: Comparison of Train Loss for Baseline and CMPE Models.

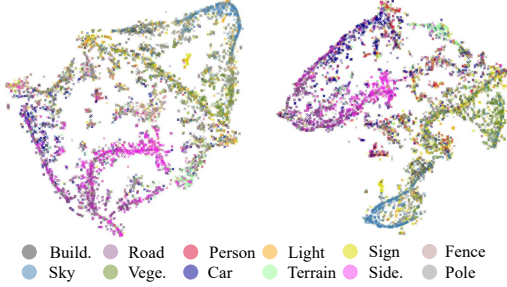


Figure 6: t-SNE embeddings of the feature space. **Left:** original source-domain dataset. **Right:** our **Vireo** after adaptation on *Cityscapes* → *ACDC* + *BDD 100k* + *Mapillary*. Each point is coloured by its semantic class.

**CLIP (ViT-L) [54]**

Fine-tune	Trainable Params*	mIoU			Avg.
		Citys	BDD	Map	
Full	304.15M	51.3	47.6	54.3	51.1
Freeze	0.00M	53.7	48.7	55.0	52.4
REIN	2.99M	57.1	54.7	60.5	57.4
FADA	11.65M	58.7	55.8	62.1	58.9
<b>Vireo (Ours)</b>	3.78M	<b>60.5</b>	<b>57.5</b>	<b>64.1</b>	<b>60.7</b>

**EVA02 (Large) [45, 46]**

Fine-tune	Trainable Params*	mIoU			Avg.
		Citys	BDD	Map	
Full	304.24M	62.1	56.2	64.6	60.9
Freeze	0.00M	56.5	53.6	58.6	56.2
REIN	2.99M	65.3	60.5	64.9	63.6
FADA	11.65M	66.7	<b>61.9</b>	66.1	64.9
<b>Vireo (Ours)</b>	3.78M	<b>68.5</b>	<b>62.1</b>	<b>67.4</b>	<b>66.0</b>

Table 6: Performance comparison of **Vireo** across multiple VFMs under the *GTA5* → *Citys.* + *BDD.* + *Map.* setting. \*Trainable parameters in backbone. Top three results are **best**, **second**, **third**. (%)

foreground masks; compared with baselines, Vireo’s focus is tighter on scene structure and semantic boundaries, explaining its consistent advantage in cross-domain and open-vocabulary settings.

**t-SNE Visualization of DGSS Features.** The feature distributions of the original dataset and our method are visualized in Figure 6, revealing the superiority of our learned features in forming well-separated semantic clusters. This demonstrates the effectiveness of our domain-generalized visual-textual alignment in structuring the open-vocabulary semantic space.

## 5 Conclusion

This study introduces Vireo, the first single-stage framework that unifies open-vocabulary recognition and domain-generalised semantic segmentation. By integrating frozen visual foundation models, depth-aware geometry and three core modules—GeoText Prompts, Coarse Mask Prior Embedding and the DOV Vector Embedding Head—it converges faster, concentrates attention on scene structure and outperforms state-of-the-art methods across multiple benchmarks, demonstrating the power of combining textual cues with geometric priors for robust pixel-level perception.

**Limitations** Vireo assumes a reliable RGB camera, but in rare cases (e.g., occlusion, glare, hardware failure), the stream can be lost, impairing perception. Future work will explore multi-source setups—automatically switching to lidar, radar, or event-based cameras when RGB fails—to keep segmentation robust in all conditions.

Configurations	Snow	Night	Fog	Rain	BDD.	Map.
REIN [35]	70.6	55.9	79.5	72.5	63.5	74.0
+ concat $f_i^d$	70.8	56.1	79.4	72.8	63.6	74.2
+ Prompt Depth Anything	70.4	55.5	79.7	72.0	63.8	73.9
+ Depth Anything V2	71.5	56.7	80.5	73.3	64.4	74.5
+ DA + AO	72.2	57.4	80.9	74.2	65.1	75.0
+ DOV-VEH	70.9	56.2	79.8	72.8	63.7	74.2
+ CMPE	71.6	56.9	80.2	73.4	64.1	74.6
+ GeoText Prompts	74.0	58.4	81.1	74.8	65.3	75.3
<b>Vireo</b>	76.2	60.6	82.3	76.3	66.7	76.0

Table 5: Ablation studies on component configurations of the proposed **Vireo** under the *Citys.* → *ACDC* with *Snow*, *Night*, *Fog*, *Rain* + *BDD.* + *Map.* generalization setting. Top three results are highlighted as **best**, **second**, and **third** (%).

**SAM (Huge) [55]**

Fine-tune	Trainable Params*	mIoU			Avg.
		Citys	BDD	Map	
Full	632.18M	57.6	51.7	61.5	56.9
Freeze	0.00M	57.0	47.1	58.4	54.2
REIN	4.51M	59.6	52.0	62.1	57.9
FADA	16.59M	61.0	53.2	63.4	60.0
<b>Vireo (Ours)</b>	5.30M	<b>64.5</b>	<b>59.0</b>	<b>66.0</b>	<b>63.2</b>

**DINOv2 (Large) [53]**

Fine-tune	Trainable Params*	mIoU			Avg.
		Citys	BDD	Map	
Full	304.20M	63.7	57.4	64.2	61.7
Freeze	0.00M	63.3	56.1	63.9	61.1
REIN	2.99M	66.4	60.4	66.1	64.3
FADA	11.65M	68.2	62.0	68.1	66.1
<b>Vireo (Ours)</b>	3.78M	<b>70.7</b>	<b>62.9</b>	<b>69.6</b>	<b>67.7</b>

## References

- [1] F. Liang, B. Wu, X. Dai, K. Li, Y. Zhao, H. Zhang, P. Zhang, P. Vajda, and D. Marculescu, “Open-vocabulary semantic segmentation with mask-adapted clip,” in *Proceedings of the IEEE/CVF conference on computer vision and pattern recognition*, 2023, pp. 7061–7070.
- [2] J. Qin, J. Wu, P. Yan, M. Li, R. Yuxi, X. Xiao, Y. Wang, R. Wang, S. Wen, X. Pan *et al.*, “Freeseq: Unified, universal and open-vocabulary image segmentation,” in *Proceedings of the IEEE/CVF Conference on Computer Vision and Pattern Recognition*, 2023, pp. 19 446–19 455.
- [3] B. Xie, J. Cao, J. Xie, F. S. Khan, and Y. Pang, “Sed: A simple encoder-decoder for open-vocabulary semantic segmentation,” in *Proceedings of the IEEE/CVF conference on computer vision and pattern recognition*, 2024, pp. 3426–3436.
- [4] C. Han, Y. Zhong, D. Li, K. Han, and L. Ma, “Open-vocabulary semantic segmentation with decoupled one-pass network,” in *Proceedings of the IEEE/CVF International Conference on Computer Vision*, 2023, pp. 1086–1096.
- [5] Y. Benigim, S. Roy, S. Essid, V. Kalogeiton, and S. Lathuilière, “Collaborating foundation models for domain generalized semantic segmentation,” in *Proceedings of the IEEE/CVF Conference on Computer Vision and Pattern Recognition*, 2024, pp. 3108–3119.
- [6] Z. Wei, L. Chen, Y. Jin, X. Ma, T. Liu, P. Ling, B. Wang, H. Chen, and J. Zheng, “Stronger fewer & superior: Harnessing vision foundation models for domain generalized semantic segmentation,” in *Proceedings of the IEEE/CVF conference on computer vision and pattern recognition*, 2024, pp. 28 619–28 630.
- [7] J. Niemeijer, M. Schwonberg, J.-A. Termöhlen, N. M. Schmidt, and T. Fingscheidt, “Generalization by adaptation: Diffusion-based domain extension for domain-generalized semantic segmentation,” in *Proceedings of the IEEE/CVF Winter Conference on Applications of Computer Vision*, 2024, pp. 2830–2840.
- [8] Q. Bi, J. Yi, H. Zheng, H. Zhan, Y. Huang, W. Ji, Y. Li, and Y. Zheng, “Learning frequency-adapted vision foundation model for domain generalized semantic segmentation,” *Advances in Neural Information Processing Systems*, vol. 37, pp. 94 047–94 072, 2024.
- [9] S. Choi, S. Jung, H. Yun, J. T. Kim, S. Kim, and J. Choo, “Robustnet: Improving domain generalization in urban-scene segmentation via instance selective whitening,” in *CVPR*, 2021, pp. 11 580–11 590.
- [10] S. Cho, H. Shin, S. Hong, A. Arnab, P. H. Seo, and S. Kim, “Cat-seg: Cost aggregation for open-vocabulary semantic segmentation,” in *Proceedings of the IEEE/CVF Conference on Computer Vision and Pattern Recognition*, 2024, pp. 4113–4123.
- [11] H. Luo, J. Bao, Y. Wu, X. He, and T. Li, “Segclip: Patch aggregation with learnable centers for open-vocabulary semantic segmentation,” in *International Conference on Machine Learning*. PMLR, 2023, pp. 23 033–23 044.
- [12] Z. Wu, X. Wu, X. Zhang, L. Ju, and S. Wang, “Siamdoge: Domain generalizable semantic segmentation using siamese network,” in *European Conference on Computer Vision*. Springer, 2022, pp. 603–620.
- [13] D. Peng, Y. Lei, M. Hayat, Y. Guo, and W. Li, “Semantic-aware domain generalized segmentation,” in *Proceedings of the IEEE/CVF conference on computer vision and pattern recognition*, 2022, pp. 2594–2605.
- [14] M. Caron, H. Touvron, I. Misra, H. Jégou, J. Mairal, P. Bojanowski, and A. Joulin, “Emerging properties in self-supervised vision transformers,” in *Proceedings of the IEEE/CVF international conference on computer vision*, 2021, pp. 9650–9660.
- [15] M. Oquab, T. Darcet, T. Moutakanni, H. Vo, M. Szafraniec, V. Khalidov, P. Fernandez, D. Haziza, F. Massa, A. El-Nouby *et al.*, “Dinov2: Learning robust visual features without supervision,” *arXiv preprint arXiv:2304.07193*, 2023.
- [16] A. Radford, J. W. Kim, C. Hallacy, A. Ramesh, G. Goh, S. Agarwal, G. Sastry, A. Askell, P. Mishkin, J. Clark *et al.*, “Learning transferable visual models from natural language supervision,” in *International conference on machine learning*. PmLR, 2021, pp. 8748–8763.
- [17] L. Yang, B. Kang, Z. Huang, X. Xu, J. Feng, and H. Zhao, “Depth anything: Unleashing the power of large-scale unlabeled data,” in *Proceedings of the IEEE/CVF Conference on Computer Vision and Pattern Recognition*, 2024, pp. 10 371–10 381.
- [18] L. Yang, B. Kang, Z. Huang, Z. Zhao, X. Xu, J. Feng, and H. Zhao, “Depth anything v2,” *Advances in Neural Information Processing Systems*, vol. 37, pp. 21 875–21 911, 2024.
- [19] S. Chen, T. Han, C. Zhang, J. Su, R. Wang, Y. Chen, Z. Wang, and G. Cai, “Hspformer: Hierarchical spatial perception transformer for semantic segmentation,” *IEEE Transactions on Intelligent Transportation Systems*, 2025.

- [20] T. Han, S. Chen, C. Li, Z. Wang, J. Su, M. Huang, and G. Cai, “Epurate-net: Efficient progressive uncertainty refinement analysis for traffic environment urban road detection,” *IEEE Transactions on Intelligent Transportation Systems*, 2024.
- [21] S. Chen, T. Han, C. Zhang, X. Luo, M. Wu, G. Cai, and J. Su, “Stronger, steadier & superior: Geometric consistency in depth vfm forges domain generalized semantic segmentation,” *arXiv preprint arXiv:2504.12753*, 2025.
- [22] B. Li, K. Q. Weinberger, S. Belongie, V. Koltun, and R. Ranftl, “Language-driven semantic segmentation,” *arXiv preprint arXiv:2201.03546*, 2022.
- [23] C. Zhou, C. C. Loy, and B. Dai, “Extract free dense labels from clip,” in *European Conference on Computer Vision*. Springer, 2022, pp. 696–712.
- [24] J. Xu, S. Liu, A. Vahdat, W. Byeon, X. Wang, and S. De Mello, “Open-vocabulary panoptic segmentation with text-to-image diffusion models,” in *Proceedings of the IEEE/CVF Conference on Computer Vision and Pattern Recognition*, 2023, pp. 2955–2966.
- [25] J. Hoffman, E. Tzeng, T. Park, J.-Y. Zhu, P. Isola, K. Saenko, A. Efros, and T. Darrell, “Cycada: Cycle-consistent adversarial domain adaptation,” in *International conference on machine learning*. Pmlr, 2018, pp. 1989–1998.
- [26] R. Volpi, H. Namkoong, O. Sener, J. C. Duchi, V. Murino, and S. Savarese, “Generalizing to unseen domains via adversarial data augmentation,” *Advances in neural information processing systems*, vol. 31, 2018.
- [27] Y. Ganin, E. Ustinova, H. Ajakan, P. Germain, H. Larochelle, F. Laviolette, M. March, and V. Lempitsky, “Domain-adversarial training of neural networks,” *Journal of machine learning research*, vol. 17, no. 59, pp. 1–35, 2016.
- [28] S. Choi, S. Jung, H. Yun, J. T. Kim, S. Kim, and J. Choo, “Robustnet: Improving domain generalization in urban-scene segmentation via instance selective whitening,” in *CVPR*, 2021, pp. 11 580–11 590.
- [29] Q. Yu, J. He, X. Deng, X. Shen, and L.-C. Chen, “Convolutions die hard: Open-vocabulary segmentation with single frozen convolutional clip,” *Advances in Neural Information Processing Systems*, vol. 36, pp. 32 215–32 234, 2023.
- [30] X. Shan, D. Wu, G. Zhu, Y. Shao, N. Sang, and C. Gao, “Open-vocabulary semantic segmentation with image embedding balancing,” in *Proceedings of the IEEE/CVF Conference on Computer Vision and Pattern Recognition*, 2024, pp. 28 412–28 421.
- [31] X. Pan, P. Luo, J. Shi, and X. Tang, “Two at once: Enhancing learning and generalization capacities via ibn-net,” in *ECCV*, 2018, pp. 464–479.
- [32] S. Lee, H. Seong, S. Lee, and E. Kim, “Wildnet: Learning domain generalized semantic segmentation from the wild,” in *CVPR*, 2022, pp. 9936–9946.
- [33] J. Ding, N. Xue, G.-S. Xia, B. Schiele, and D. Dai, “Hgformer: Hierarchical grouping transformer for domain generalized semantic segmentation,” in *CVPR*, 2023, pp. 15 413–15 423.
- [34] Q. Bi, S. You, and T. Gevers, “Learning content-enhanced mask transformer for domain generalized urban-scene segmentation,” in *AAAI*, vol. 38, no. 2, 2024, pp. 819–827.
- [35] Z. Wei, L. Chen, Y. Jin, X. Ma, T. Liu, P. Ling, B. Wang, H. Chen, and J. Zheng, “Stronger fewer & superior: Harnessing vision foundation models for domain generalized semantic segmentation,” in *CVPR*, 2024, pp. 28 619–28 630.
- [36] Q. Bi, J. Yi, H. Zheng, H. Zhan, Y. Huang, W. Ji, Y. Li, and Y. Zheng, “Learning frequency-adapted vision foundation model for domain generalized semantic segmentation,” *NeurIPS*, vol. 37, pp. 94 047–94 072, 2024.
- [37] M. Cordts, M. Omran, S. Ramos, T. Rehfeld, M. Enzweiler, R. Benenson, U. Franke, S. Roth, and B. Schiele, “The cityscapes dataset for semantic urban scene understanding,” in *CVPR*, 2016, pp. 3213–3223.
- [38] F. Yu, H. Chen, X. Wang, W. Xian, Y. Chen, F. Liu, V. Madhavan, and T. Darrell, “Bdd100k: A diverse driving dataset for heterogeneous multitask learning,” in *CVPR*, 2020, pp. 2636–2645.
- [39] G. Neuhold, T. Ollmann, S. Rota Bulò, and P. Kontschieder, “The mapillary vistas dataset for semantic understanding of street scenes,” in *ICCV*, 2017, pp. 4990–4999.
- [40] C. Sakaridis, D. Dai, and L. Van Gool, “Acdc: The adverse conditions dataset with correspondences for semantic driving scene understanding,” in *ICCV*, 2021, pp. 10 745–10 755.
- [41] B. Zhou, H. Zhao, X. Puig, T. Xiao, S. Fidler, A. Barriuso, and A. Torralba, “Semantic understanding of scenes through the ade20k dataset,” *International Journal of Computer Vision*, vol. 127, no. 3, pp. 302–321, 2019.



- [42] S. R. Richter, V. Vineet, S. Roth, and V. Koltun, “Playing for data: Ground truth from computer games,” in *ECCV*. Springer, 2016, pp. 102–118.
- [43] J. Zhang, R. Liu, H. Shi, K. Yang, S. Reiß, K. Peng, H. Fu, K. Wang, and R. Stiefelhagen, “Delivering arbitrary-modal semantic segmentation,” in *CVPR*, 2023.
- [44] M. Contributors, “MMSegmentation: Openmmlab semantic segmentation toolbox and benchmark,” <https://github.com/open-mmlab/mms Segmentation>, 2020.
- [45] Y. Fang, W. Wang, B. Xie, Q. Sun, L. Wu, X. Wang, T. Huang, X. Wang, and Y. Cao, “Eva: Exploring the limits of masked visual representation learning at scale,” in *CVPR*, 2023, pp. 19 358–19 369.
- [46] Y. Fang, Q. Sun, X. Wang, T. Huang, X. Wang, and Y. Cao, “Eva-02: A visual representation for neon genesis,” *arXiv preprint arXiv:2303.11331*, 2023.
- [47] Z. Zhong, Y. Zhao, G. H. Lee, and N. Sebe, “Adversarial style augmentation for domain generalized urban-scene segmentation,” *NeurIPS*, vol. 35, pp. 338–350, 2022.
- [48] P. Chattopadhyay, K. Sarangmath, V. Vijaykumar, and J. Hoffman, “Pasta: Proportional amplitude spectrum training augmentation for syn-to-real domain generalization,” in *ICCV*, 2023, pp. 19 288–19 300.
- [49] D. Peng, Y. Lei, L. Liu, P. Zhang, and J. Liu, “Global and local texture randomization for synthetic-to-real semantic segmentation,” *IEEE TIP*, vol. 30, pp. 6594–6608, 2021.
- [50] E. J. Hu, Y. Shen, P. Wallis, Z. Allen-Zhu, Y. Li, S. Wang, L. Wang, and W. Chen, “Lora: Low-rank adaptation of large language models,” *arXiv preprint arXiv:2106.09685*, 2021.
- [51] S. Chen, C. Ge, Z. Tong, J. Wang, Y. Song, J. Wang, and P. Luo, “Adaptformer: Adapting vision transformers for scalable visual recognition,” *NeurIPS*, vol. 35, pp. 16 664–16 678, 2022.
- [52] M. Jia, L. Tang, B.-C. Chen, C. Cardie, S. Belongie, B. Hariharan, and S.-N. Lim, “Visual prompt tuning,” in *ECCV*. Springer, 2022, pp. 709–727.
- [53] M. Oquab, T. Darcet, T. Moutakanni, H. Vo, M. Szafraniec, V. Khalidov, P. Fernandez, D. Haziza, F. Massa, A. El-Nouby *et al.*, “Dinov2: Learning robust visual features without supervision,” *arXiv preprint arXiv:2304.07193*, 2023.
- [54] A. Radford, J. W. Kim, C. Hallacy, A. Ramesh, G. Goh, S. Agarwal, G. Sastry, A. Askell, P. Mishkin, J. Clark *et al.*, “Learning transferable visual models from natural language supervision,” in *International conference on machine learning*. PmLR, 2021, pp. 8748–8763.
- [55] A. Kirillov, E. Mintun, N. Ravi, H. Mao, C. Rolland, L. Gustafson, T. Xiao, S. Whitehead, A. C. Berg, W.-Y. Lo *et al.*, “Segment anything,” in *ICCV*, 2023, pp. 4015–4026.
- [56] M. Xu, Z. Zhang, F. Wei, Y. Lin, Y. Cao, H. Hu, and X. Bai, “A simple baseline for open-vocabulary semantic segmentation with pre-trained vision-language model,” in *European Conference on Computer Vision*. Springer, 2022, pp. 736–753.
- [57] G. Ghiasi, X. Gu, Y. Cui, and T.-Y. Lin, “Scaling open-vocabulary image segmentation with image-level labels,” in *European conference on computer vision*. Springer, 2022, pp. 540–557.
- [58] X. Zou, Z.-Y. Dou, J. Yang, Z. Gan, L. Li, C. Li, X. Dai, H. Behl, J. Wang, L. Yuan *et al.*, “Generalized decoding for pixel, image, and language,” in *Proceedings of the IEEE/CVF conference on computer vision and pattern recognition*, 2023, pp. 15 116–15 127.
- [59] J. Xu, S. De Mello, S. Liu, W. Byeon, T. Breuel, J. Kautz, and X. Wang, “Groupvit: Semantic segmentation emerges from text supervision,” in *Proceedings of the IEEE/CVF conference on computer vision and pattern recognition*, 2022, pp. 18 134–18 144.
- [60] H. Zhang, F. Li, X. Zou, S. Liu, C. Li, J. Yang, and L. Zhang, “A simple framework for open-vocabulary segmentation and detection,” in *Proceedings of the IEEE/CVF International Conference on Computer Vision*, 2023, pp. 1020–1031.
- [61] Q. Huang, H. Hu, and J. Jiao, “Revisit the open nature of open vocabulary segmentation,” in *Thirteenth International Conference on Learning Representations*, 2025.
- [62] D. Li, J. Yang, K. Kreis, A. Torralba, and S. Fidler, “Semantic segmentation with generative models: Semi-supervised learning and strong out-of-domain generalization,” in *Proceedings of the IEEE/CVF conference on computer vision and pattern recognition*, 2021, pp. 8300–8311.
- [63] W.-J. Ahn, G.-Y. Yang, H.-D. Choi, and M.-T. Lim, “Style blind domain generalized semantic segmentation via covariance alignment and semantic consistence contrastive learning,” in *Proceedings of the IEEE/cvf conference on computer vision and pattern recognition*, 2024, pp. 3616–3626.
- [64] H. Niu, L. Xie, J. Lin, and S. Zhang, “Exploring semantic consistency and style diversity for domain generalized semantic segmentation,” in *Proceedings of the AAAI Conference on Artificial Intelligence*, vol. 39, no. 6, 2025, pp. 6245–6253.

## Appendix / Supplemental Material

### A Open Source Dataset and Experiments

To advance research in real-world open-vocabulary and domain-generalized semantic segmentation, we introduce **AustinScapes**, a new large-scale street-view dataset collected from the city of Austin, Texas, USA. The dataset comprises 100,000 high-resolution street-level images, each accompanied by pixel-level semantic annotations. The annotation schema follows the Cityscapes 19-class labels, ensuring compatibility with existing benchmarks.

AustinScapes captures a wide variety of urban scenes under diverse lighting, architectural styles, and traffic conditions, making it well-suited for evaluating both fine-grained recognition and robustness across real-world complexities. We benchmark our method and previous state-of-the-art approaches on AustinScapes to assess generalization performance. Figure 8 shows the visualization results of DGSS and OVSS methods on the AustinScapes dataset. Experimental results show that our framework maintains superior segmentation quality, particularly in challenging object categories and under domain shifts, further validating its effectiveness on unseen urban domains.

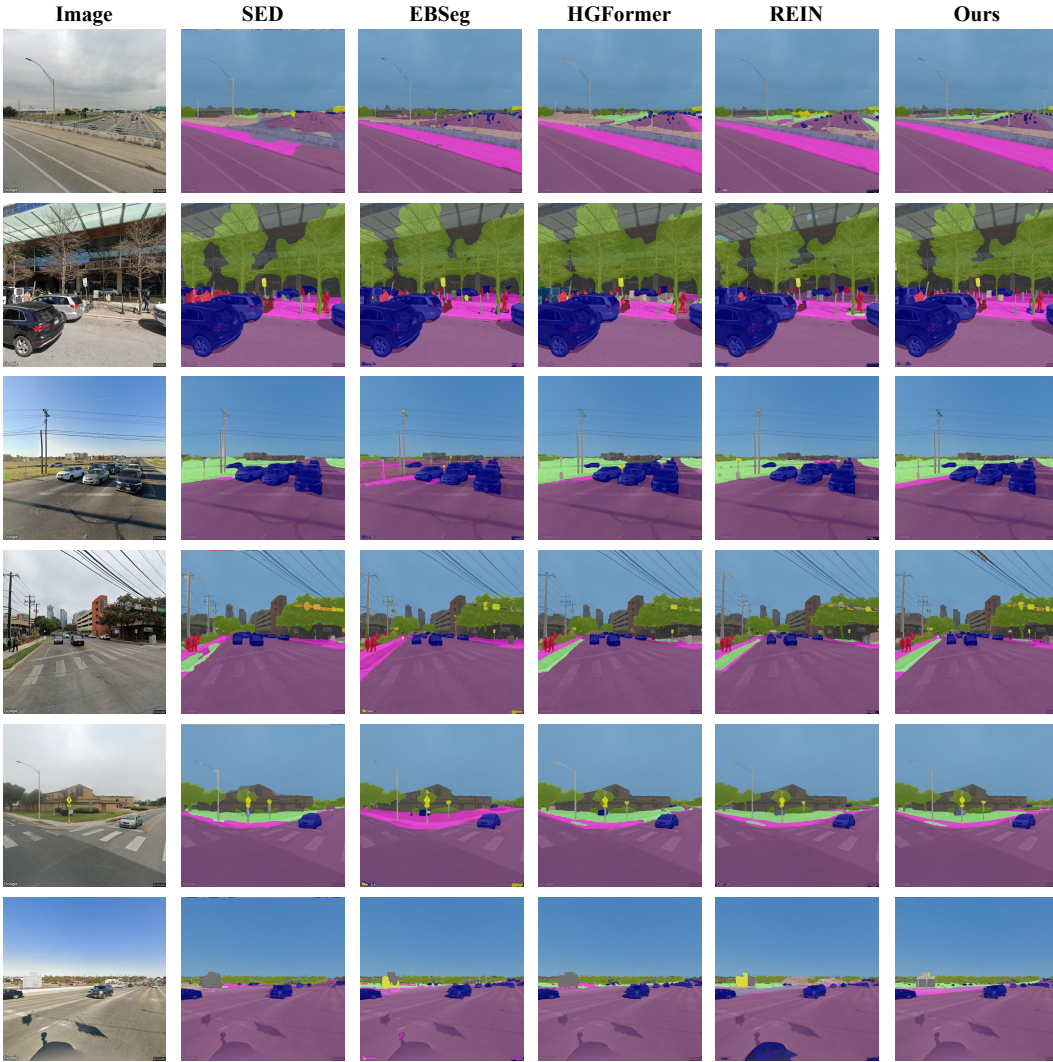


Figure 8: Key zero-shot segmentation examples from existing DGSS and OVSS methods, and our Vireo, on the AustinScapes dataset.

## B Related Works

This section provides a more comprehensive discussion of the research areas that are highly relevant to our work: Open-Vocabulary Semantic Segmentation (OVSS) and Domain-Generalized Semantic Segmentation (DGSS). By examining these areas, we aim to highlight our contributions in bridging the gap between DGSS and OVSS.

### B.1 Open-Vocabulary Semantic Segmentation

Existing OVSS methods [24, 10, 30, 3] primarily leverage the rich semantic knowledge embedded in pre-trained vision-language models (VLMs) such as CLIP [54]. Early approaches often adopt two-stage pipelines. For example, ZSSeg [56] classifies class-agnostic masks using CLIP, and MaskCLIP [23] adapts CLIP for instance mask proposal classification. Towards end-to-end solutions, LSeg [22] generates pixel-level embeddings aligned with text features, and OVSeg [1] further enhances this by learning discriminative pixel embeddings using a class-agnostic decoder. OpenSeg [57] presents a unified, language-driven framework for open-vocabulary segmentation.

To reduce dependency on region proposals, FreeSeg [2] introduces a grouping-based strategy to cluster pixels. Generalized decoders such as X-Decoder [58] enable language-conditioned pixel-level predictions. GroupViT [59] explores hierarchical region grouping with textual concepts. SegCLIP [11], a task-specific adaptation, enhances spatial understanding from CLIP for dense prediction tasks. More recently, OpenSeeD [60] aims to unify multiple segmentation tasks under the open-vocabulary setting via a conditioned decoder, and Cat-seg [10] improves multimodal matching by jointly modeling image and text in the cost function. Additionally, [61] addresses evaluation issues by proposing a mask-matching-based framework to handle semantic ambiguity.

Despite these advances, challenges remain in transferring coarse-grained VLM knowledge to pixel-level predictions and in resolving fine-grained linguistic ambiguities. Our work builds upon this line of research by incorporating depth cues to enhance language-guided segmentation, particularly in disambiguating objects within complex scenes.

### B.2 Domain-Generalized Semantic Segmentation

Previous methods primarily focus on learning feature representations that are both discriminative for semantic segmentation and invariant to domain-specific variations. A foundational strategy in DGSS is introduced by DANN [27], which employs adversarial training with a domain classifier. Li et al. [62] investigate generative approaches using GANs to model the joint distribution of images and labels, while RobustNet [28] mitigates domain-specific biases through instance-selective whitening. SAN-SAW [13] introduces semantic-aware normalization using SAN and SAW modules, and BlindNet [63] enhances robustness by disentangling style and content representations.

More recently, pre-trained VLMs have been effectively leveraged in DGSS frameworks [8, 6, 64, 5]. These methods utilize frozen VLM features as universal backbones and optimize learnable tokens to improve cross-domain performance.

Building upon these advancements, our work posits that integrating the semantic generality of language with the geometric stability of depth provides a compelling approach to achieving robust domain-generalized open-vocabulary segmentation.

## C Expend Experiments and Analysis

In this section, we present per-class method comparisons, model details, and visual results that are excluded from the main manuscript owing to page constraints.

### C.1 More Data Analysis and Model Details

From Table 7, our approach achieves a mIoU of 66.73%, significantly outperforming other OVSS approaches. Compared to the second-best SED (48.16% mIoU), this represents an improvement of 18.57 percentage points, demonstrating a substantial enhancement in cross-domain generalization. Moreover, our approach attains the best performance in 18 categories.

Table 7: Performance comparison across OVSS methods on per-class IoU and mIoU (City.→BDD.). Top three results are highlighted as **best**, **second**, and **third**, respectively(%).

Method	road	side.	build.	wall	fence	pole	light	sign	vege	terr.	sky	pers.	rider	car	truck	bus	train	moto.	bicy.	mIoU
EBseg	89.72	42.47	81.24	25.11	31.24	45.95	40.14	44.32	80.57	17.67	93.20	50.52	24.96	83.97	35.60	62.83	0.00	39.60	40.02	40.59
FC-CLIP	93.63	57.06	79.53	18.63	38.78	48.86	24.17	48.45	83.89	45.27	83.26	69.16	55.44	88.55	44.13	75.35	0.00	66.74	<b>60.34</b>	51.41
CAT-Seg	92.08	50.94	79.41	29.08	38.85	13.88	25.88	28.88	79.26	44.20	91.11	45.51	30.07	82.74	40.65	64.85	0.00	43.23	36.18	44.28
SED	93.78	60.35	82.90	30.07	44.48	39.26	44.97	46.22	83.40	45.55	92.53	60.06	29.23	86.92	43.64	42.94	0.31	43.88	42.12	48.16
Ours	<b>95.40</b>	<b>68.08</b>	<b>88.29</b>	<b>34.81</b>	<b>46.11</b>	<b>60.95</b>	<b>62.31</b>	<b>59.80</b>	<b>87.26</b>	<b>51.10</b>	<b>95.27</b>	<b>72.94</b>	<b>62.63</b>	<b>90.93</b>	<b>53.82</b>	<b>83.08</b>	<b>22.35</b>	<b>74.40</b>	58.37	<b>66.73</b>

Table 8: Comparison of per-class IoU across OVSS methods on the DELIVER dataset. Top three results are highlighted as **best**, **second**, and **third**, respectively(%).

Class	Cloud					Fog					Night					Rain					Sun				
	Ours	SED	CAT-Seg	FC-CLIP	EBseg	Ours	SED	CAT-Seg	FC-CLIP	EBseg	Ours	SED	CAT-Seg	FC-CLIP	EBseg	Ours	SED	CAT-Seg	FC-CLIP	EBseg	Ours	SED	CAT-Seg	FC-CLIP	EBseg
Building	73.71	81.43	81.63	53.96	81.64	52.58	64.43	59.10	50.79	62.79	56.24	77.20	74.99	58.13	75.90	57.34	72.25	79.73	60.24	71.22	85.55	83.17	81.47	49.24	84.39
Fence	39.24	18.22	25.89	28.31	29.54	37.52	14.10	19.50	25.53	21.56	21.20	7.07	10.65	12.99	8.94	38.06	11.77	16.88	24.36	20.86	37.10	10.67	23.77	22.65	28.26
Other	0.00	0.00	0.00	0.11	0.04	0.00	0.00	0.00	0.02	0.06	0.00	0.00	0.00	0.00	0.13	0.00	0.00	0.00	0.00	0.17	0.00	0.00	0.00	1.88	0.03
Pedestrian	68.86	39.43	21.84	4.21	16.64	73.61	36.72	14.02	2.96	36.21	56.44	31.99	9.00	8.78	5.93	66.21	33.65	19.85	3.28	17.14	64.61	30.83	13.25	3.37	23.59
Pole	32.17	19.50	15.62	6.74	31.35	31.91	21.96	17.90	5.82	35.65	24.20	20.46	14.19	6.51	33.20	32.85	26.89	20.69	6.69	34.53	37.35	22.33	19.39	4.20	34.08
RoadLine	0.00	5.87	2.30	4.46	2.95	0.00	5.44	2.28	3.94	1.30	0.00	5.09	1.94	3.59	2.68	0.00	5.63	2.11	4.01	2.38	0.00	4.80	2.09	3.96	3.02
Road	91.70	29.72	89.55	0.00	65.80	91.72	24.25	89.15	0.01	80.96	90.78	26.22	86.28	0.00	64.23	91.65	32.11	88.48	0.01	67.85	91.94	22.69	88.78	0.00	63.06
SideWalk	71.50	57.22	57.36	59.27	59.04	66.91	53.90	55.25	47.48	43.27	69.18	56.95	58.65	54.13	38.89	69.50	56.40	56.95	52.37	45.44	71.16	48.96	55.14	44.70	27.36
Vegetation	69.36	61.11	62.12	29.30	39.67	68.58	58.86	58.96	33.79	35.20	38.46	40.39	31.46	24.22	20.33	66.69	62.29	62.37	28.17	31.89	68.85	58.12	59.30	54.17	68.62
Cars	63.84	60.20	57.84	66.49	65.73	68.99	60.90	58.78	72.55	68.84	77.26	66.19	60.66	74.09	67.51	64.80	59.94	53.38	62.80	60.64	70.38	65.32	59.65	66.64	64.05
Wall	3.46	0.08	2.05	2.67	4.14	0.30	0.00	0.00	0.08	0.43	2.11	1.46	0.00	1.47	1.53	0.47	0.41	0.01	0.49	0.23	4.07	5.95	0.00	0.29	3.80
TrafficSign	22.00	26.99	25.02	30.59	23.55	32.28	36.64	24.98	10.11	25.88	20.83	35.63	33.87	12.18	26.76	13.01	28.84	26.61	14.26	20.98	32.60	41.36	42.29	29.98	32.87
Sky	86.90	92.22	94.09	26.28	59.90	67.51	82.47	82.87	18.12	41.63	43.22	79.51	56.92	21.98	7.81	65.98	77.80	92.65	11.00	13.61	96.37	95.20	95.22	23.70	97.22
Ground	0.00	0.01	0.00	0.00	0.01	0.00	0.00	0.00	0.00	0.00	0.00	0.05	0.00	0.00	0.00	0.00	0.00	0.07	0.00	0.00	0.00	0.00	0.00	0.00	0.00
Bridge	0.00	0.00	0.15	0.00	0.00	0.00	0.00	0.11	0.00	0.00	0.00	0.00	0.04	0.13	0.00	0.00	0.00	0.01	0.03	0.00	0.00	0.00	0.29	0.00	0.00
RailTrack	0.06	0.00	0.00	0.00	0.00	0.00	0.00	0.00	0.00	0.21	0.00	0.00	0.00	0.00	0.00	0.06	0.00	0.00	0.00	0.25	0.00	0.00	0.00	0.00	0.00
GroundRail	0.00	12.80	0.00	15.07	0.00	0.00	8.32	0.03	11.33	0.00	0.00	11.20	0.00	6.31	0.00	0.00	6.93	0.00	8.85	0.00	0.00	6.72	0.00	11.54	0.00
TrafficLight	57.73	25.71	23.39	24.94	13.05	67.39	41.82	29.52	10.24	21.85	51.48	30.92	21.47	2.01	4.45	58.03	23.86	22.72	4.60	10.50	61.49	39.72	25.74	3.17	17.78
Static	0.00	0.07	0.00	0.12	0.00	0.00	0.01	0.01	0.00	0.22	0.00	0.01	0.00	0.00	0.00	0.00	0.00	0.01	0.00	0.00	0.00	0.04	0.02	0.00	0.00
Dynamic	0.00	0.00	0.00	0.01	0.36	0.00	0.00	0.00	0.00	0.06	0.00	0.00	0.00	0.00	0.53	0.00	0.00	0.00	0.01	0.18	0.00	0.00	0.00	0.00	0.78
Water	0.00	0.00	0.00	0.00	0.00	0.00	0.00	0.00	0.00	0.00	0.00	0.00	0.00	0.68	0.00	0.00	0.00	0.38	0.00	0.00	0.00	0.00	0.00	0.00	0.00
Terrain	48.31	32.42	38.57	15.22	4.35	45.35	27.11	35.20	17.08	2.42	37.71	13.06	28.41	4.41	0.45	47.53	25.24	33.96	17.23	9.46	43.44	25.18	31.03	15.49	5.16
TwoWheeler	51.66	37.99	16.31	20.55	12.10	60.03	41.90	22.45	29.29	11.42	48.04	31.61	14.29	25.50	13.74	68.66	52.24	41.47	34.45	41.11	60.42	47.01	38.37	31.28	40.16
Bus	0.00	0.01	0.00	3.76	0.00	0.00	6.11	0.00	4.45	0.00	0.00	0.93	0.00	0.00	0.00	0.00	0.00	0.00	23.64	12.30	0.00	0.00	0.00	1.73	0.05
Truck	28.00	9.22	41.70	45.42	55.62	53.19	43.36	49.80	68.80	60.14	50.18	33.77	10.99	50.29	14.40	54.24	45.11	45.65	52.43	47.98	67.95	64.92	69.59	55.30	66.04
Mean	<b>33.89</b>	24.40	26.22	17.50	22.62	<b>35.80</b>	25.25	24.80	17.26	22.00	<b>29.89</b>	22.79	20.56	14.93	15.50	<b>33.46</b>	25.18	26.53	16.59	20.35	<b>38.49</b>	27.14	28.21	16.93	26.41

For small targets prone to missed detections under extreme conditions (such as traffic lights and pedestrians), our method achieves 62.31% and 72.94% (17.34% and 12.88% higher than SED), respectively. The results reflect the robustness of our method in complex scenarios.

As shown in Table 8, on the DELIVER dataset, our method achieves the highest mIoU across all five extreme weather conditions, outperforming the runner-up by an average of 8–11 percentage points. Under Sun and Cloud conditions, large classes achieve over 80% IoU. In more adverse conditions, our method still maintains IoUs above 30%. Even in the most challenging Night scenario, we outperform others by a margin of 7.10%.

For fine-grained categories such as TwoWheeler, Pedestrian, TrafficSign, and TrafficLight, our method consistently outperforms competitors, demonstrating strong recognition of low-contrast and small-scale objects. Although rare categories exhibit lower absolute IoUs, we still rank among the top in most of these cases. Overall, our approach demonstrates superior performance across both frequent and challenging classes under diverse weather conditions.

Table 9 compares training time, memory usage, FPS, inference time, and final mIoU (averaged across ACDC, BDD100K, and Mapillary) for various OVSS methods and the baseline, all evaluated under a unified 40k-iteration schedule with a batch size of 8. While Vireo’s training time (15 hours 2 minutes) and inference time (43 minutes) are not the shortest, it achieves the highest mIoU of 73.0%, utilizing 18.4 GB of memory at 1.36 FPS, substantially outperforming all other approaches.

Importantly, we follow the previous configuration of intermediate DINOv2 feature layers ( $\{\hat{f}_i^V\}_{i=1}^4, l_i \in \{8, 12, 16, 24\}$ ), which has been demonstrated in prior work to offer an optimal

Table 9: Efficiency and Performance Comparison

Method	Iter.	Train (4 BS)	Mem.	FPS	Infer.	Perform.
SED	40k	6h59min	20.8G	1.73	33min	57.0%
CAT-Seg	40k	3h3min	9.7G	1.66	35min	48.9%
FC-CLIP	40k	5h34min	18.7G	1.45	40min	58.7%
EBSeg	40k	6h34min	22.1G	0.62	94min	49.7%
REIN	40k	12h6min	13.8G	1.88	31min	69.4%
Vireo	40k	15h2min	18.4G	1.49	39min	73.0%



trade-off between accuracy and efficiency. This ensures a fair and consistent comparison across all methods in our experiments.

## C.2 More Visualization Results

Figure 9 presents a visual comparison of segmentation results between DGSS methods and ours on the *Cityscapes*  $\rightarrow$  *ACDC* target domain. The first row shows the original outputs, while the second and third rows display zoomed-in crops for closer inspection. In the original images, other models clearly miss regions on the left sidewalk. In the second-row crops, our method yields much finer and more complete boundaries around small objects such as traffic lights and signs, detecting nearly every instance. In the third-row crops, even distant vehicles and signals are accurately segmented. Moreover, Vireo maintains continuous, clean segmentation of roads and sidewalks in low-contrast conditions (nighttime, rain, snow), without breaks or noise artifacts. It preserves highly consistent segmentation across large background areas like sky, buildings, and vegetation, suppressing “speckle” noise. It precisely captures very fine structures such as curbs and road markings. And it produces coherent, complete contours for dynamic objects (pedestrians, cyclists, vehicles). Whether in clear daytime or foggy, rainy nighttime scenarios, Vireo demonstrates superior cross-scenario robustness.

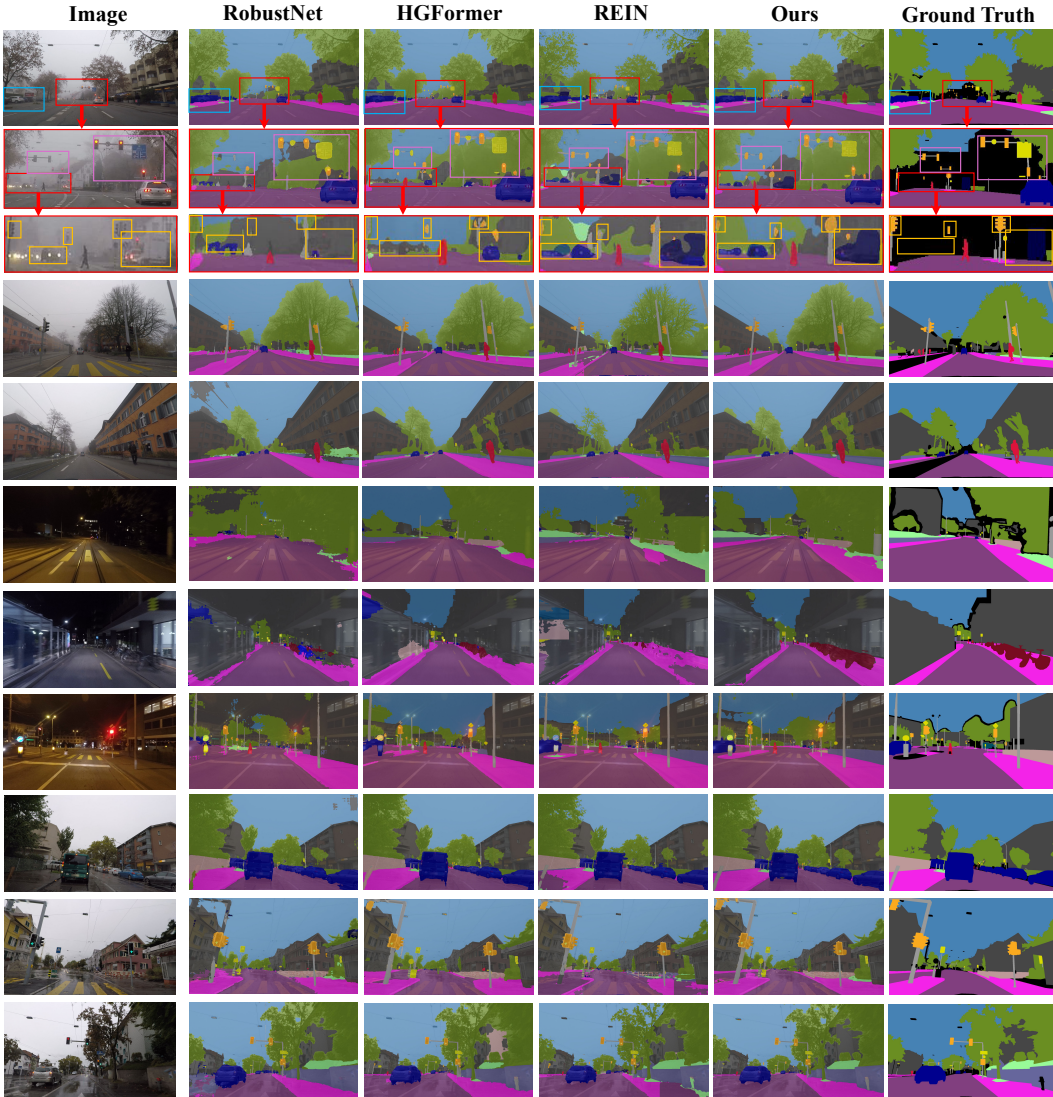


Figure 9: Key segmentation examples of existing DGSS methods and Vireo under the Cityscapes  $\rightarrow$  ACDC unseen target domains under Night, Snow, Rain, and Fog conditions.



Figure 10 presents a visual comparison of segmentation results between DGSS methods and ours on the *GTA5*  $\rightarrow$  *Cityscapes* + *BDD* + *Mapillary* target domains. Across these varying scene distributions, RobustNet, HGFormer, and REIN often misclassify or omit road markings, crosswalks, clusters of pedestrians, and parked vehicles. In contrast, our Vireo consistently preserves the complete contours of dynamic objects and slender structures (e.g., lampposts, traffic signals). It segments curbs and lane lines continuously without breaks and delineates building–sky boundaries more sharply. It renders vegetation and other background regions with uniform, noise-free color blocks. Even for distant groups of pedestrians or in highly cluttered street scenes, Vireo accurately separates adjacent classes. This further demonstrates its superior generalization and robustness to unseen domains.



Figure 10: Key segmentation examples of existing DGSS methods and Vireo under the *GTA5* $\rightarrow$ *City.*, *BDD.* and *Map.* unseen target domains.

Figure 11 presents a comparison of segmentation results between various OVSS methods and Vireo on the *Cityscapes*  $\rightarrow$  *ACDC* target domain. The first column shows the original input images, followed by CAT-Seg, EBSeg, FC-CLIP, SED, Vireo, and finally the ground truth. As observed, CAT-Seg and EBSeg often yield fragmented road and sidewalk segmentations with background noise under extreme conditions such as rain, snow, and nighttime. FC-CLIP partially recovers large objects but still fails to detect small targets like traffic lights and thin poles. SED shows some improvement in road continuity but struggles with distant small objects and background consistency. In contrast, Vireo consistently produces continuous, precise segmentations of roads, lane markings, pedestrians, vehicles, and traffic signals across all weather and lighting conditions. It maintains low-noise, highly uniform background regions. Its outputs most closely match the ground truth, further demonstrating Vireo’s superior performance and robustness in open-vocabulary, cross-domain scenarios.



Figure 11: Key segmentation examples of existing OVSS methods and Vireo under the *Cityscapes*  $\rightarrow$  *ACDC* unseen target domains under Night, Snow, Rain, and Fog conditions.

Figure 12 compares OVSS methods and our Vireo on the *Cityscapes*  $\rightarrow$  *DELIVER* transfer setting, which includes sunny, rainy, cloudy, foggy, and nighttime conditions. FC-CLIP preserves mask edges but suffers from widespread class errors. CAT-Seg and EBSeg yield fragmented road and sidewalk masks with spurious background artifacts under adverse conditions. SED improves overall continuity but still missegments slender structures like poles and signs in low-contrast scenarios. In contrast, Vireo consistently produces clear, coherent masks for zebra crossings, lane markings, sidewalks, pedestrians, vehicles, and poles. It effectively suppresses noise in sky, building, and vegetation regions. The outputs most closely match the ground truth, demonstrating superior robustness and generalization in extreme, unseen domains.

As shown in Figure 13, adding CMPE and GTP transforms the attention from a diffuse pattern into a concentrated focus on critical regions such as roads, vehicles, and pedestrians. In the Affinity Map, bright clusters reveal the model’s ability to capture long-range dependencies within the same object, while dark boundaries emphasize clear separation between different semantic regions. Together, these results confirm our method’s robust handling of semantic coherence and pixel-level affinities across diverse weather and lighting conditions.

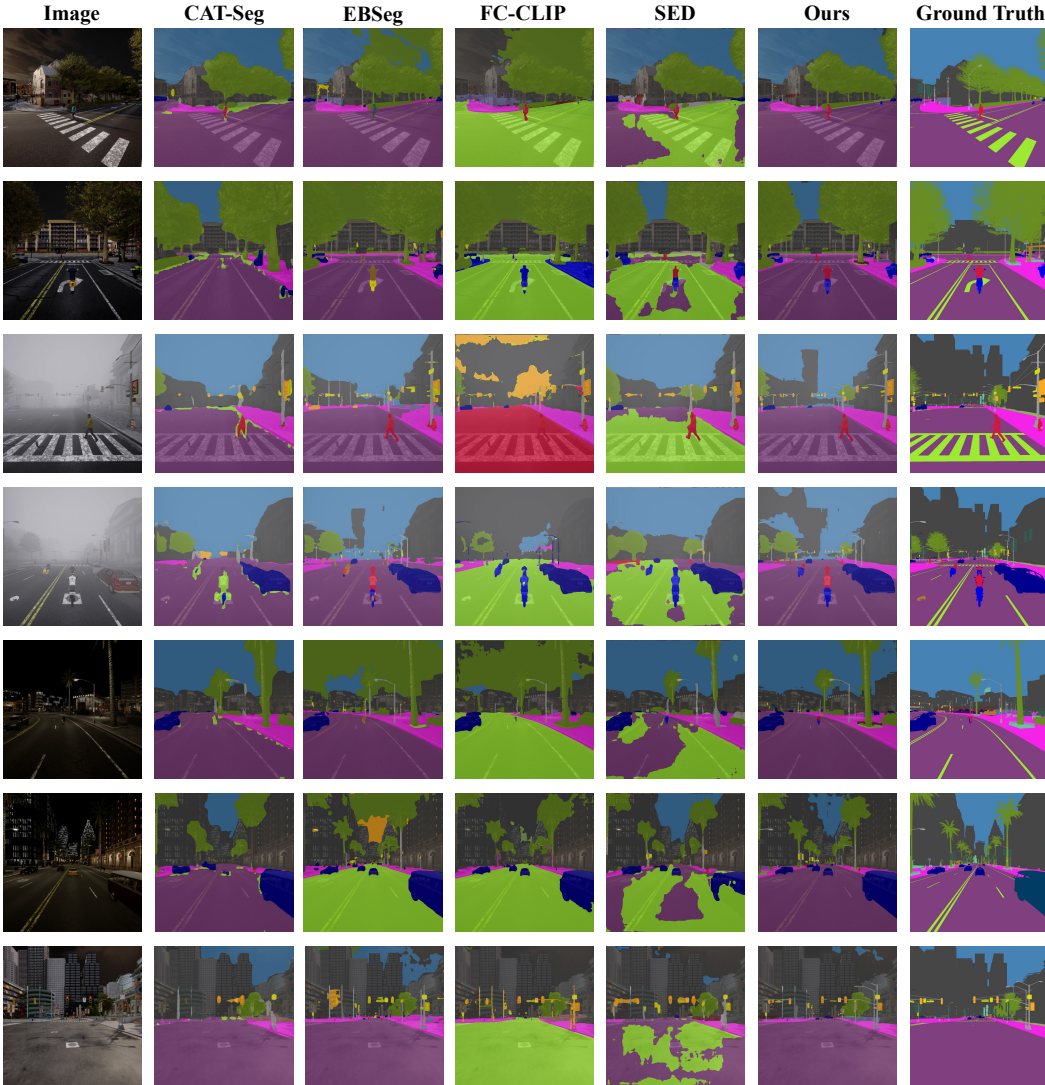


Figure 12: Key segmentation examples of existing OVSS methods and Vireo under the *Citysc.*  $\rightarrow$  *DELIVER* unseen target domains under Cloud, Fog, Night, Rain, and Sun conditions.



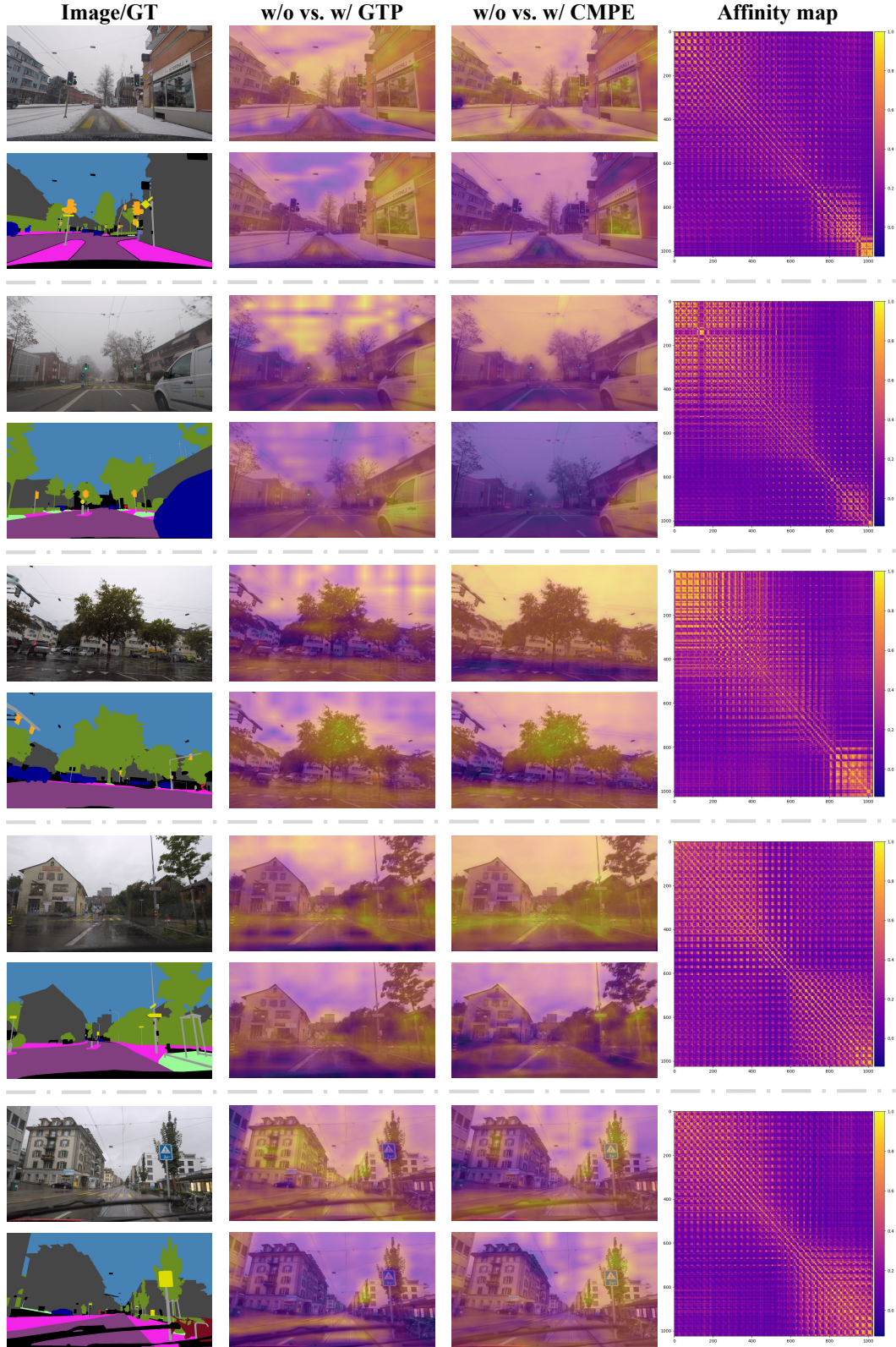


Figure 13: Visualizations of attention maps and affinity maps under different scenes, where CMPE denotes the Coarse Mask Prior Embedding and GTP represents the GeoText Prompts.